Chinese Journal of Chemical Engineering 65 (2024) 1–7

Contents lists available at ScienceDirect

Chinese Journal of Chemical Engineering

journal homepage: www.elsevier.com/locate/CJChE

Full Length Article

Flower-like tin oxide membranes with robust three-dimensional channels for efficient removal of iron ions from hydrogen peroxide

Risheng Shen [1,#], Shilong Li [1,#], Yuqing Sun [1], Yuan Bai [2], Jian Lu [1], Wenheng Jing [1,*]

[1] State Key Laboratory of Materials-Oriented Chemical Engineering, Nanjing Tech University, Nanjing 210009, China
[2] National Energy Group Science and Technology Research Institute Co., Ltd., Nanjing 210023, China

ARTICLE INFO

Article history:
Received 3 April 2023
Received in revised form 15 August 2023
Accepted 17 August 2023
Available online 23 August 2023

Keywords:
Hydrogen peroxide
SnO_2 membrane
Adsorption
Hydrothermal

ABSTRACT

Membrane technology has become the mainstream process for the production of electronic grade hydrogen peroxide (H_2O_2). But due to the oxidation degradation of the organic membranes (*e.g.* polyamide) by the strong oxidative radicals (*e.g.* ·OH) generated *via* the activation of H_2O_2 by iron ions (Fe^{3+}), the short effective lifetime of membranes remains a challenge. Inorganic nano tin oxide (SnO_2) has great potential for the removal of Fe^{3+} in strongly oxidative H_2O_2 because of its ability to stabilize H_2O_2 and preferentially adsorb Fe^{3+}. Herein, we have designed for the first time a flower-like robust SnO_2 membrane on the ceramic support by *in situ* template-free one-step hydrothermal method. The three-dimensional loose pore structure in the membrane built by interlacing SnO_2 nanosheets endows the SnO_2 membrane with a high specific surface area and abundant adsorption sites (—OH). Based on the coordination complexation and electrostatic attraction between the SnO_2 surface and Fe^{3+}, the membrane shows a high Fe^{3+} removal efficiency (83%) and permeability (24 $L{\cdot}m^{-2}{\cdot}h^{-1}{\cdot}MPa^{-1}$) in H_2O_2. This study provides an innovative and simple approach to designing robust SnO_2 membranes for highly efficient removal of Fe^{3+} in harsh environments, such as strong oxidation conditions.

1. Introduction

Electronic grade hydrogen peroxide is widely used in the electronics industry, for example as a cleaning agent for silicon wafers [1]. The deposition of trace metal ions (Fe^{3+}, Ca^{2+}, K^+, Na^+, *etc.*) in H_2O_2 on the surface of silicon wafers can adversely affect the electrical properties of silicon devices [2], it requires ultra-purification processes, such as distillation, adsorption, ion exchange, membrane technologies, *etc.*, to achieve electronic grade requirements [3]. Because no auxiliary chemicals are required and zero effluent is generated, membrane technologies (mainly polyamide membranes) become the most desirable ultra-purification option. However, polyamide membranes can only maintain stability for three days when exposed to H_2O_2 degradation, which is directly evidenced by an increase in permeate flux and a decrease in rejection levels [4]. One of the main reasons for the degradation is the ·OH radicals generated by the activation of Fe^{3+} through the Fenton reaction [5–7]. In order to extend the effective lifetime of reverse osmosis membranes and reduce the operation cost of H_2O_2 ultra purification, developing a robust membrane capable of Fe^{3+} removal in advance under oxidizing conditions is of great significance.

Inorganic metal oxide ceramic materials (such as zirconia and tin dioxide) are often researched as an adsorbent to remove Fe^{3+} in H_2O_2 due to their high anti-oxidation, heavy metal ion adsorption ability, and chemical tolerance [8,9]. The construction of two-dimensional (2D) and three-dimensional (3D) tin oxide (SnO_2) morphologies has attracted much more attention as it can possess higher specific surface area and surface adsorption activity, exhibiting better reactivity toward various applications such as photocatalysis [10], sensing [11], separation [12], *etc.* Benefiting from abundant adsorption sites and negatively charged properties, SnO_2 is often used for the removal of molecules and ions [13–15].

In this study, a flower-like SnO_2 membrane can be constructed to gain the coordination complexation and electrostatic attraction between the SnO_2 surface and Fe^{3+} by *in situ* template-free one-step hydrothermal method for the first time, to realize H_2O_2 stabilization and preferentially Fe^{3+} adsorbing capacity. Thin nanosheets and the 3D channels structure create a high specific surface area and abundant adsorption sites (—OH). A high removal efficiency (83%) of Fe^{3+} is achieved by the combined action of coordination complexation and electrostatic attraction.

* Corresponding author.
E-mail address: jingwh@njtech.edu.cn (W. Jing).
# These authors contributed equally to this work.

https://doi.org/10.1016/j.cjche.2023.08.002

2. Experimental

2.1. Synthesis of SnO_2 nanosheets

SnO_2 nanosheets were prepared using a "bottom-up" approach with direct hydrothermal [16,17]. Specifically, 6 mmol·L^{-1} $SnCl_2{\cdot}2H_2O$ (98%, Aladdin, China) was quickly dissolved in a 20 ml aqueous solution containing 5 ml anhydrous ethanol and 15 ml deionized (DI) water to form a precursor solution of SnO_2 by stirring. Then, 45 ml 0.5 mol·L^{-1} NaOH (98%, Aladdin, China) solution was slowly added to the solution. The obtained mixture was transferred into a 100 ml Teflon-lined stainless autoclave and set the filling volume of the solution to 25%, 50%, 75%, 85%, and 95% respectively, sealed and maintained at 150 °C for 12 h, and then cooled down to room temperature. The precipitates were obtained by centrifuge and washed several times with water and ethanol respectively until Cl^- could not be detected. The products were dried in the vacuum at 60 °C for 2 h.

2.2. Preparation of flower-like SnO_2 ceramic membrane

The flower-like SnO_2 ceramic membrane was obtained using a one-step growth method (Fig. 1). Porous α-Al_2O_3 disks (Membrane Science & Technology Research Center, China: 30 mm in diameter, 3 mm in thickness, 0.1 μm in average pore size) with robust mechanical stability were used as supports where the SnO_2 crystals grow. The other side of the support was covered by Teflon tape to prevent the crystals from growing. It was placed in the precursor solution synthesized in Section 2.1 for 12 h at 150 °C. Then the membrane was removed and rinsed in fresh ethanol for several hours, and dried at 60 °C.

2.3. Characterization

The morphology of SnO_2 nanosheets and element composition of SnO_2 membranes were characterized by field emission scanning electron microscopy (FESEM, S-4800, Hitachi, Japan) equipped with the energy dispersive spectrometer (EDX). X-ray diffraction (XRD, D8 Advance, Bruker, Germany) was conducted to qualitatively identify crystalline phases and quantitatively characterize the d-spacing of SnO_2 membranes. The nitrogen adsorption–desorption isotherms of SnO_2 nanosheets and SnO_2 nanoparticles were measured on an ASAP 2460 (Micromeritics, America) at −196 °C. The multipoint Brunner–Emmet–Teller (BET) method was carried out to calculate the specific surface area of the prepared material in the P/P_0 range of 0.05–0.25 and Barrett–Joyner–Halenda (BJH) was used to measure the corresponding pore diameter, pore volume at P/P_0 of 0.995. The zeta potential of the SnO_2 membrane was characterized by a Zetasizer (ZS90, Malvern, England). All metal ions were analyzed by inductively coupled plasma optical emission spectrometer (ICP–OES, Ametek, India). Fourier transforms infrared (FTIR, Thermo Nicolet8700, America) spectroscopy was used to identify chemical bonds in the SnO_2 and Fe^{3+} using a Spectrum GX spectrometer (PerkinElmer, America) with a KBr pellet operating in transmittance mode. X-ray photoelectron spectroscopy (XPS, Thermo Kalpha, America) was recorded on an ESCALAB 250Xi.

A self-designed device with cross-flow conditions (Fig. S1, in Supplementary Material) was used to test the permeance and the solute removal efficiency. The feed solution was fed continuously using a plunger pump at a pressure between 0.1 and 1.0 MPa. The feed liquid was 0.4 mg·L^{-1} Fe^{3+} aqueous solution and 30% H_2O_2 (AR, Yonghuachem, China), respectively, and the concentration of Fe^{3+} was 0.06 mg·L^{-1} in H_2O_2. The counter ion of Fe ion is Cl ion ($c(Cl^-)$ = 0.76 mg·L^{-1}) and the pH of 0.4 mg·L^{-1} Fe ion solution simulated 30% H_2O_2 solution, pH = 3.6. The feed temperature was maintained at 25 °C. The retentate was recycled back to the feed container, and the permeate was at atmospheric pressure. The permeance (J, L·m^{-2}·h^{-1}·MPa^{-1}) and the solute removal efficiency R (%) were calculated based on the following equations:

$$J = V/(A \times t \times P) \tag{1}$$

$$R = (1 - C_P/C_F) \times 100\% \tag{2}$$

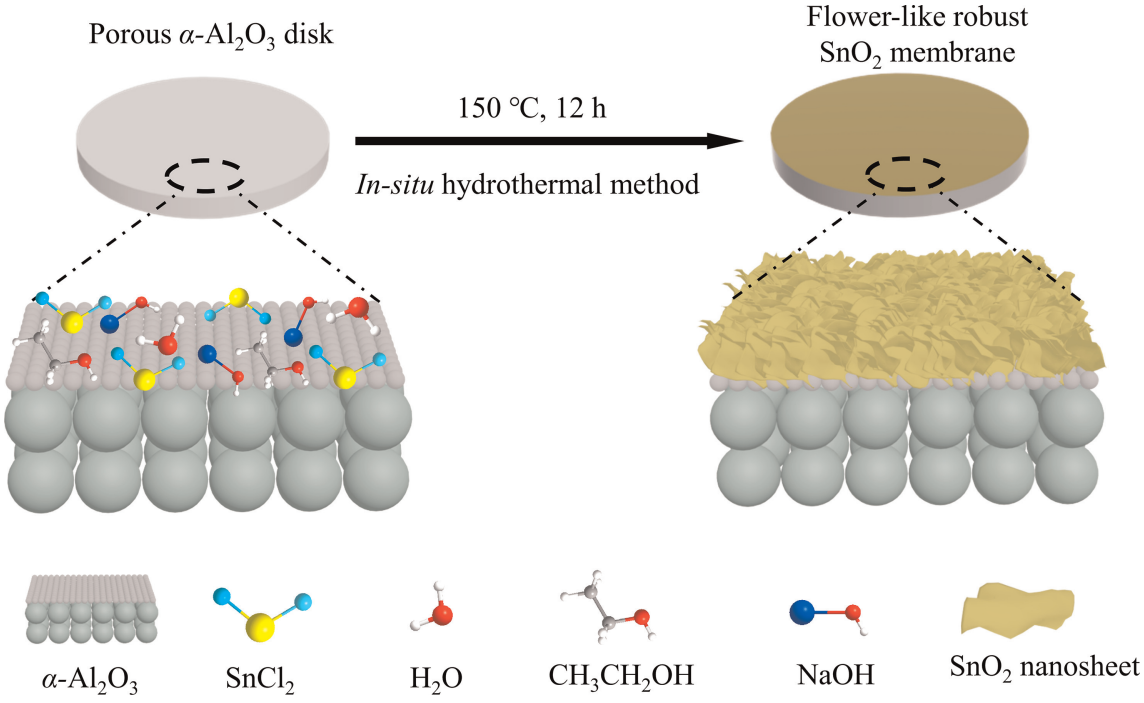

Fig. 1. Schematic illustration of the one-step *in situ* hydrothermal synthesis of SnO_2 membranes.

In Eq. (1), V (L) represents permeation volume, A (m^2) is the corresponding effective membrane filtration area, t (h) represents the filtration time, P (MPa) is the permeation pressure; In Eq. (2), C_P and C_F represent the solute concentrations of permeation and feed solution, respectively.

3. Results and Discussion

3.1. Characterization of SnO_2 nanosheets

The morphology and purity of SnO_2 are influenced by the level of filling in the kettle liquid, as different filling levels correspond to different pressures and oxygen levels. The pressure corresponding to different filling levels is measured using an autoclave with a pressure gauge. The pressures are 0.25, 0.3, 0.4, 0.5 and 0.6 MPa for 25%, 50%, 75%, 85% and 95% fill levels respectively. In this work, five filler levels are set up to investigate the effect on the morphology and purity of the nanosheets. FESEM investigates the general morphologies of the prepared SnO_2 materials, and the results are demonstrated in Fig. 2. As shown in Fig. 2(a) and (b), the SnO_2 is presented as nanoparticles and did not form nanosheets. It may attribute to the low pressure in the kettle causing the seed crystals to dissolve and not grow. Increasing the pressure, SnO_2 nanosheets are successfully prepared (Fig. 2(c)–(e)). It possesses spreading flower-shaped morphologies and very high density (Fig. 2(b)). Interestingly, it is observed that the flower-shaped structures,

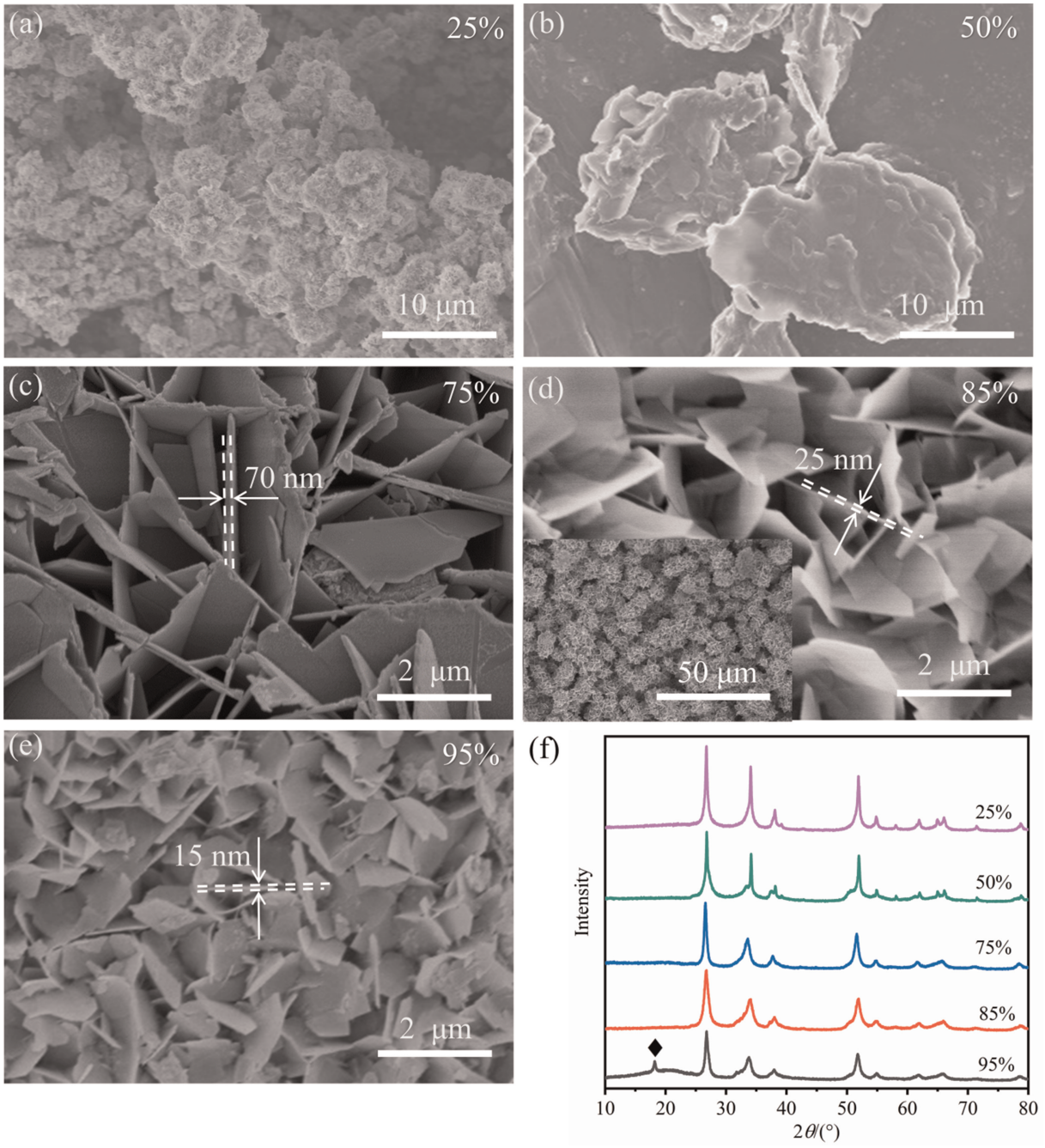

Fig. 2. The SEM images (a–e) and XRD patterns (f) of SnO_2 nanosheets in the filling level of the kettle liquid to 25%, 50%, 75%, 85%, and 95% respectively.

almost triangular-shaped, are made of thin nanosheets which intermingle with each other in such a manner that one corner of individual nanosheet is connected with the side surface of the nanosheet (Fig. 2(c)–(e)). This particular structure may be related to the oriented attachment of the crystal [18]. The fast oriented attachment of the SnO_2 nanoparticles results in the formation of SnO_2 nanosheets. Subsequently, because of the surface energy minimization, the newly formed nanoparticles would spontaneously land on the as-formed sheets and preferential further grow to another nanosheet in the [0 0 1] direction, thus flower-like SnO_2 architectures are formed [19,20]. The thickness of the nanosheets becomes thinner with increasing fill levels, 70, 25, and 15 nm respectively.

To examine the crystallinity and crystal phases, the prepared SnO_2 is analyzed by the XRD pattern. Fig. 2(f) shows the XRD patterns of the prepared SnO_2 nanosheets. The first four groups of identified peaks can be indexed to SnO_2 with a tetragonal rutile structure (JCPDF 41-1445). Except for SnO_2, no other diffraction reflections are detected in the pattern, which confirms that the prepared samples are well crystalline and pure SnO_2. The broadening of the peaks with increasing filling indicates a reduction in grain size, further suggesting that the synthesized products are nanoscale microcrystals. However, at a filling level of 95%, the characteristic (0 0 1) peak of SnO locates at 2θ = 18.27°, which is attributed to the insufficient amount of oxygen in the kettle, resulting in the inability to fully oxidize the Sn^{2+} to Sn^{4+}. Considering the thickness and purity of the nanosheets, 85% is a suitable level of filling of the kettle liquid for the preparation of SnO_2 nanosheets with a high specific surface area and no impurities.

3.2. Characterization of flower-like SnO_2 membrane

The morphology of the *in-situ* hydrothermally synthesized SnO_2 membrane is shown in Fig. 3(a) and (b). The surface of the membrane is a flower-like structure (Fig. 3(a)), and the thickness of the membrane is 2.7 μm (Fig. 3(b)). By XRD characterization (Fig. 3(c)), the characteristic peaks of both Al_2O_3 and SnO_2 appear on the SnO_2 membrane, respectively, and the peak pattern is enhanced at the 2θ angle overlap of the two substances, with no impurity peaks appearing. This indicates that good crystallinity and impurity-free SnO_2 membranes are successfully prepared. Fig. 3(d) displays the polyethylene glycol (PEC) retention of the SnO_2 membrane. The molecular weight (MWCO) of the membrane is 2686 Da, according to the formula $r = 0.0262 \times M_W^{1/2} - 0.03$, and the corresponding pore size is 2.7 nm [21].

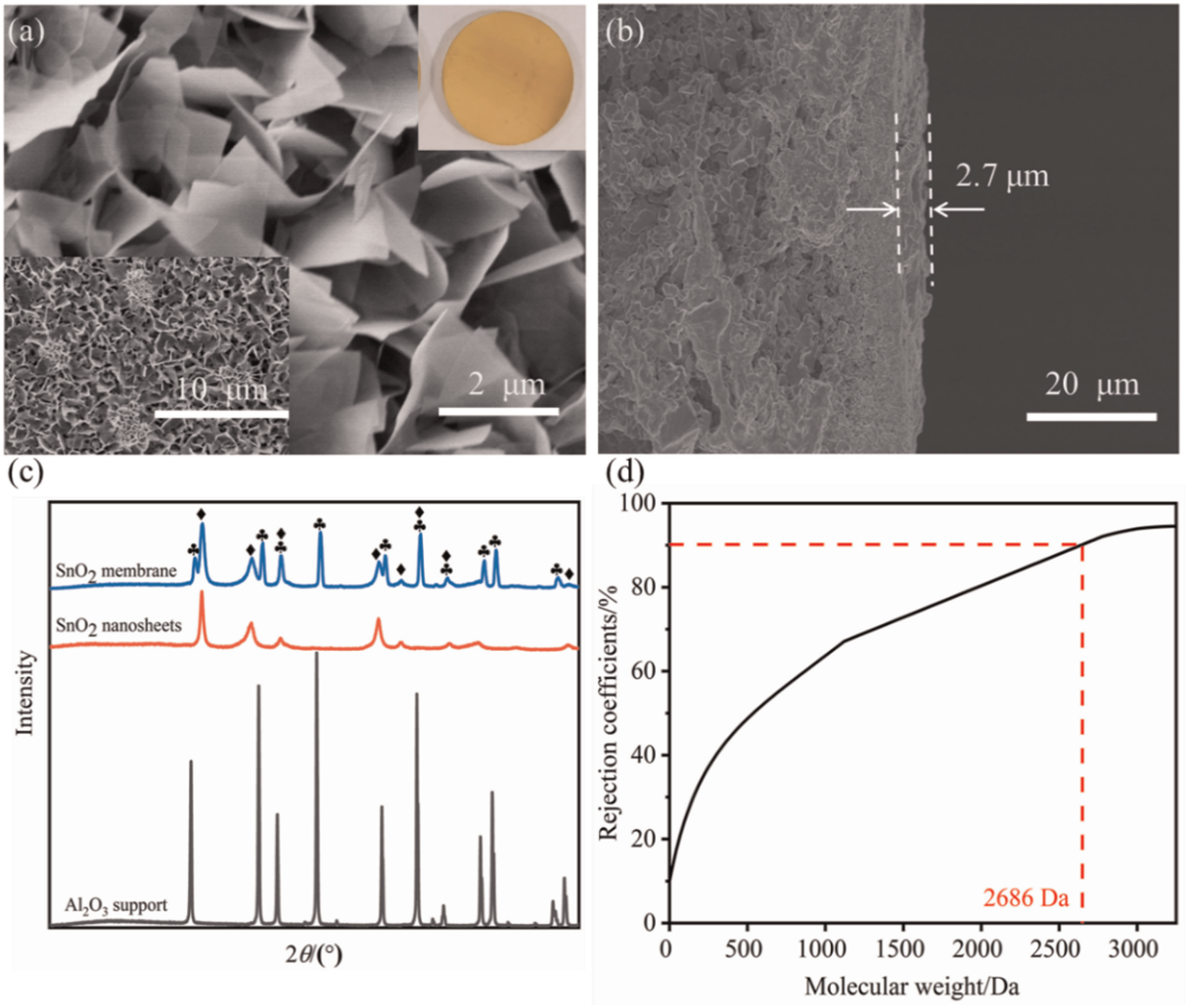

Fig. 3. The SEM images (a, b) and XRD patterns (c) of SnO_2 membrane; The PEG retention of the SnO_2 membrane (d).

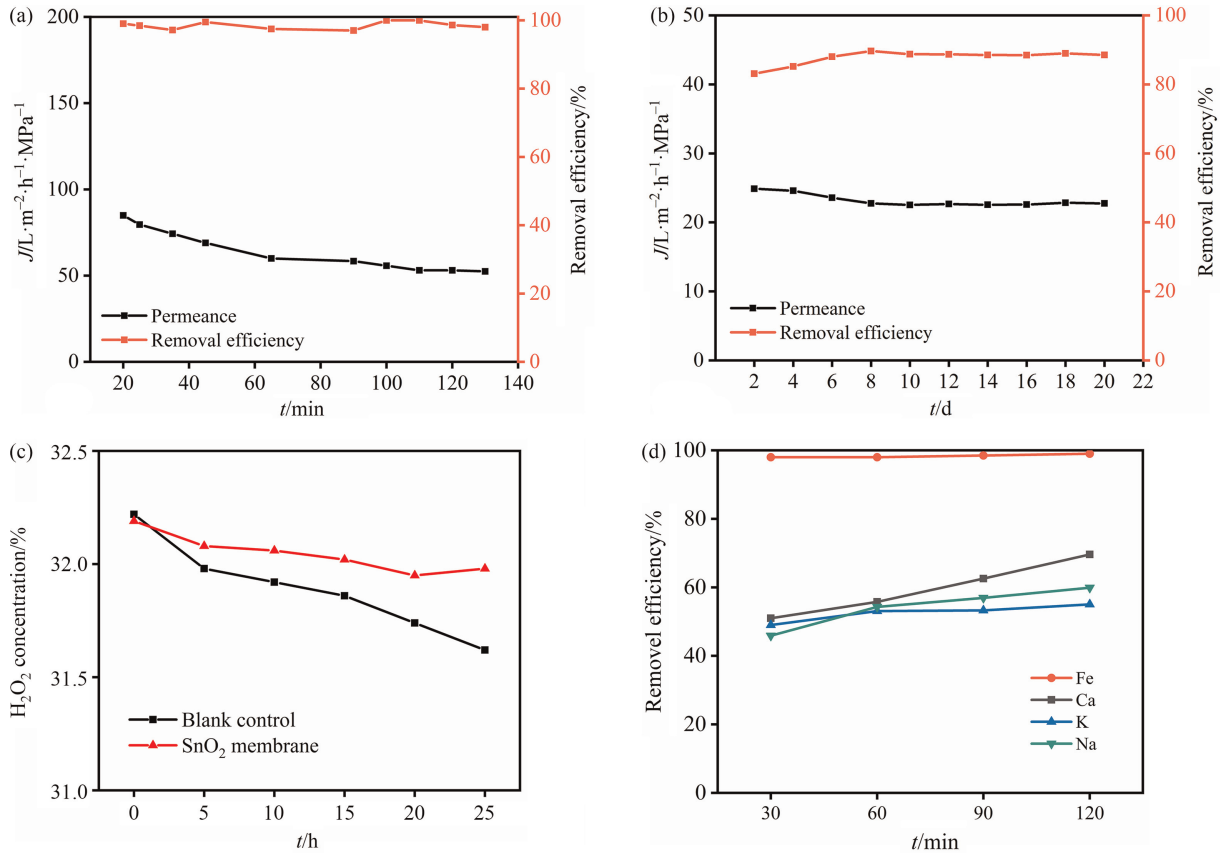

Fig. 4. The permeability and the removal efficiency of Fe^{3+} for doped water (a) and 30% H_2O_2 (b) at 0.3 MPa; effect of SnO_2 membrane on the decomposition of H_2O_2 (c); removal efficiency (d) of SnO_2 membrane for different metal ions in doped water.

3.3. Characterisation of SnO_2 membrane for Fe^{3+} removal

Fig. 4(a) and (b) shows the permeability and the removal efficiency of Fe^{3+} in doped water and H_2O_2 at 0.3 MPa. The SnO_2 membrane has a good removal effect on Fe^{3+} in doped water, with a removal rate of over 97% (Fig. 4(a)). Fig. 4(b) shows a Fe^{3+} removal efficiency (83%) and permeability (24 $L{\cdot}m^{-2}{\cdot}h^{-1}{\cdot}MPa^{-1}$) in H_2O_2. During this treatment, a layer of bronzing impurities deposit (Fig. S2(a) and (c)), and EDX characterization (Fig. S2(b)) found that the impurities were iron precipitates [4].

Considering the process safety, the compatibility of H_2O_2 and membrane materials is a prerequisite for purifying H_2O_2. Fig. 4(c) explores the compatibility of the SnO_2 membrane with H_2O_2, which shows SnO_2 membrane has an inhibitory effect on H_2O_2 decomposition. Fig. 4(d) shows the removal efficiency of the SnO_2 membrane for different metal ions, and finds that the SnO_2 membrane has priority in removing Fe^{3+}, Ca^{2+} took second place, while K^+ and Na^+ are the lowest. The preferential adsorption of Fe^{3+} may be related to its charges. Fig. S4 shows the wash-cycle stability test of the flower-shaped SnO_2 membrane. The membrane performance remained basically stable, but the adsorption residue of a small amount of impurities on the active sites on the membrane surface resulted in a slight decrease in both membrane flux and removal efficiency.

3.4. The mechanism of SnO_2 membrane for Fe^{3+} removal

The specific surface area and the porous structure of SnO_2 nanosheets are characterized by nitrogen adsorption–desorption isotherms (Fig. 5(a)). Compared to SnO_2 nanoparticles (AR, XFNANO, China) (Fig. S3), SnO_2 nanosheets show typical IV isotherms, and the hysteresis loops are of type H3 [22], associating with the slit-like shape produced by layered packing. The major pore size distribution of SnO_2 ranges from 2 to 7 nm, suggesting the formation of a typical mesoporous structure [23]. Moreover, the specific surface area of prepared SnO_2 is calculated to be 49 $m^2{\cdot}g^{-1}$, much larger than that of the SnO_2 nanoparticles (5 $m^2{\cdot}g^{-1}$). This significant increase in the specific surface area provides a large number of active sites for Fe^{3+} adsorption and enhances adsorption efficiency.

The microscopic mechanism of action needs to be explored to understand the process of removing Fe^{3+} from SnO_2 membranes. Fig. 5(b) shows the zeta potential of SnO_2 nanosheets at different pH, which reveals that SnO_2 is negatively charged at pH = 2–10. This indicates that when the feed liquid is hydrogen peroxide (pH = 3.6), the negative charge on the SnO_2 surface will allow Fe^{3+} to migrate to the surface of the material through electrostatic attraction. The higher the charge, the stronger the electrostatic attraction [23]. This mechanism explains the preferential adsorption phenomenon in Fig. 4(d). Fig. 5(c) shows the infrared spectra of SnO_2 before and after the adsorption of Fe^{3+}. It can be seen that the bending of —OH (3443 cm^{-1}) is partially weakened after the adsorption of Fe^{3+}, which could be the result of the coordination complexation between hydroxyl groups on the surface of SnO_2 and Fe^{3+}. To further explore the mechanism of the adsorption process. Fig. 5(d) exhibits the chromatogram of O 1s before and after SnO_2 adsorption in XPS characterization. After the adsorption of Fe^{3+}, Fe—O bonds appear at the corresponding position with a bond energy of 530.6 eV, indicating that Fe^{3+} are adsorbed onto SnO_2 and complexed with hydroxyl groups on SnO_2, which is consistent with infrared characterization analysis.

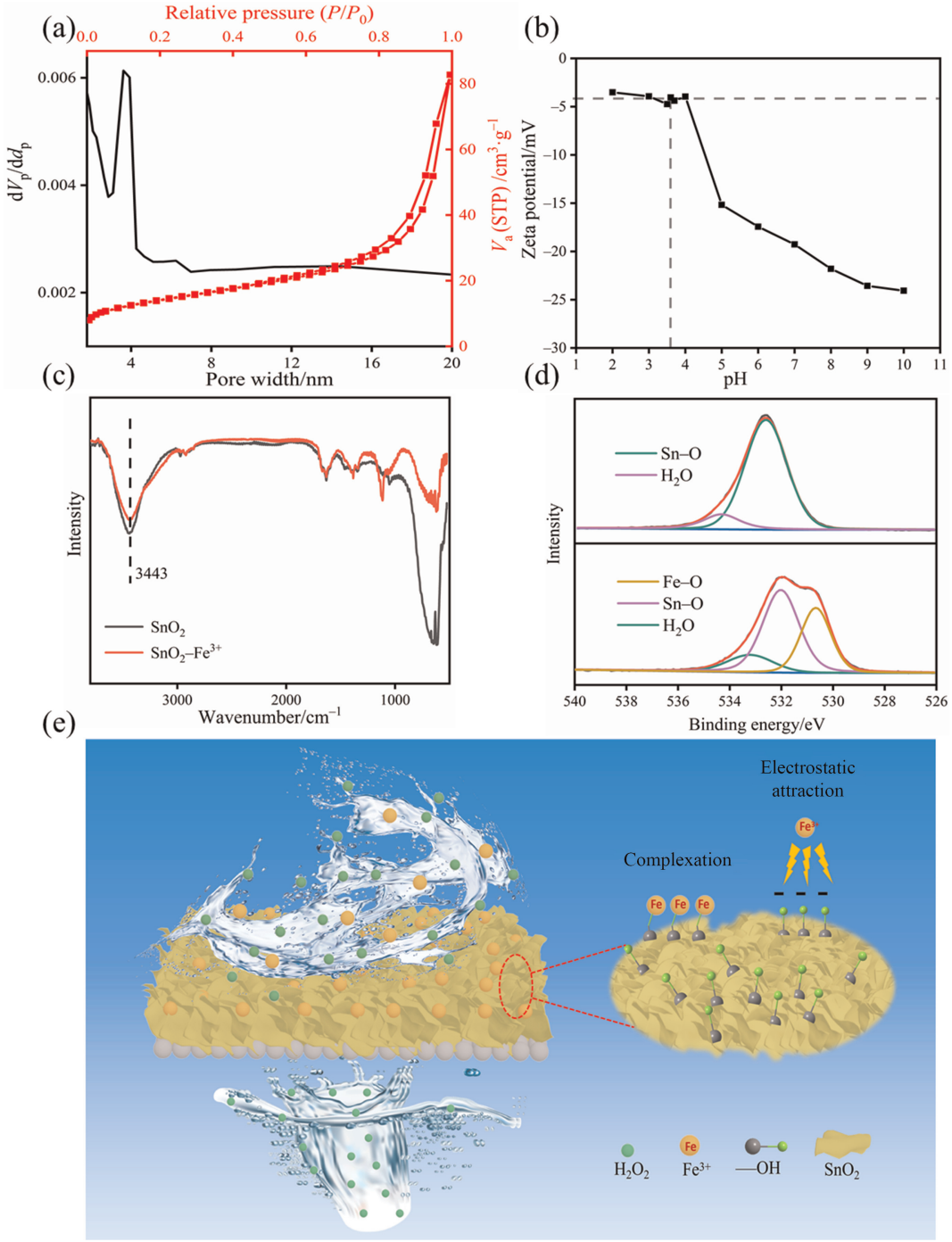

Fig. 5. Nitrogen adsorption–desorption isotherms, pore size distribution of SnO_2 nanosheets (a); zeta potential of SnO_2 nanosheets at different pH (b); FTIR spectra of SnO_2 nanosheets before and after adsorption of Fe^{3+} (c); O 1s spectra of before and after adsorption (d); microscopic mechanism diagram of adsorption (e).

Fig. 5(e) displays a microscopic mechanism diagram of adsorption. Benefiting from abundant adsorption sites (—OH) and negatively charged properties, the membranes exhibit H_2O_2 stabilization and preferentially adsorbing capacity toward Fe^{3+} based on coordination complexation and electrostatic attraction.

4. Conclusions

The synthesis of a flower-like SnO_2 ceramic membrane by *in situ* template-free one-step hydrothermal method is presented. Because of abundant adsorption sites (—OH) brought by the 3D pore structure of SnO_2 and negatively charged properties, SnO_2 membranes exhibit H_2O_2 stabilization and preferentially adsorbing capacity toward Fe^{3+} based on coordination complexation and electrostatic attraction, which could remove Fe^{3+} with a high efficiency of more than 83% and permeability (24 $L{\cdot}m^{-2}{\cdot}h^{-1}{\cdot}MPa^{-1}$) in H_2O_2. This study provides an innovative and practical approach for producing robust SnO_2 membranes with 3D channels for the highly efficient removal of Fe^{3+} in harsh environments.

CRediT Authorship Contribution Statement

Risheng Shen: Methodology, Validation, Formal analysis, Investigation, Data curation, Writing – original draft, Writing – review & editing. **Shilong Li:** Methodology, Resources, Data curation, Writing – original draft, Validation. **Yuqing Sun:** Resources, Supervision, Project administration, Funding acquisition. **Yuan Bai:** Methodology, Resources, Formal analysis. **Jian Lu:** Investigation, Validation, Formal analysis. **Wenheng Jing:** Conceptualization, Writing – review & editing, Resources, Supervision, Project administration, Funding acquisition.

Data Availability

Data will be made available on request.

Declaration of Competing Interest

The authors declare that they have no known competing financial interests or personal relationships that could have appeared to influence the work reported in this paper.

Acknowledgements

We sincerely appreciate the support from the National Key Research and Development Program (2021YFB3801303), the National Natural Science Foundation of China (21838005, 21921006), the State Key Laboratory of Materials-Oriented Chemical Engineering (SKL-MCE-22A03), and the Key Research and Development Program of Jiangsu Provincial Department of Science and Technology (BE2022033-3).

Supplementary Material

Supplementary material to this article can be found online at https://doi.org/10.1016/j.cjche.2023.08.002.

References

[1] C.W. Lan, S. Kubendhiran, G. Sison, H.P. Hsu, Monitoring hydrogen peroxide using an electrochemical method during metal assisted chemical etching for silicon, *Silicon* 14 (10) (2022) 5673–5681.
[2] R. Abejón, A. Garea, A. Irabien, Analysis, modelling and simulation of hydrogen peroxide ultrapurification by multistage reverse osmosis, *Chem. Eng. Res. Des.* 90 (3) (2012) 442–452.
[3] R. Abejón, A. Garea, A. Irabien, Ultrapurification of hydrogen peroxide solution from ionic metals impurities to semiconductor grade by reverse osmosis, *Sep. Purif. Technol.* 76 (1) (2010) 44–51.
[4] R. Abejón, A. Garea, A. Irabien, Effective lifetime study of commercial reverse osmosis membranes for optimal hydrogen peroxide ultrapurification processes, *Ind. Eng. Chem. Res.* 52 (48) (2013) 17270–17284.
[5] R. Ling, L. Yu, T.P.T. Pham, J.H. Shao, J.P. Chen, M. Reinhard, Catalytic effect of iron on the tolerance of thin-film composite polyamide reverse osmosis membranes to hydrogen peroxide, *J. Membr. Sci.* 548 (2018) 91–98.
[6] L. Yu, R. Ling, J.P. Chen, M. Reinhard, Quantitative assessment of the iron-catalyzed degradation of a polyamide nanofiltration membrane by hydrogen peroxide, *J. Membr. Sci.* 588 (2019) 117154.
[7] R. Ling, J.H. Shao, J.P. Chen, M. Reinhard, Iron catalyzed degradation of an aromatic polyamide reverse osmosis membrane by free chlorine, *J. Membr. Sci.* 577 (2019) 205–211.
[8] L. Wang, C.X. Shi, L. Wang, L. Pan, X.W. Zhang, J.J. Zou, Rational design, synthesis, adsorption principles and applications of metal oxide adsorbents: A review, *Nanoscale* 12 (8) (2020) 4790–4815.
[9] R. Shyamala, L. Gomathi Devi, Reduced graphene oxide/SnO_2 nanocomposites for the photocatalytic degradation of Rhodamine B: Preparation, characterization, photosensitization, vectorial charge transfer mechanism and identification of reaction intermediates, *Chem. Phys. Lett.* 748 (2020) 137385.
[10] L. Liu, Y.Y. Wang, Y.B. Dai, G.H. Li, S.Q. Wang, T. Li, T. Zhang, S.J. Qin, *In situ* growth of NiO@SnO_2 hierarchical nanostructures for high performance H_2S sensing, *ACS Appl. Mater. Interfaces* 11 (47) (2019) 44829–44836.
[11] D.C.O.S. Neves, A.L. da Silva, R.C. de Oliveira Romano, D. Gouvêa, Fe_2O_3-doped SnO_2 membranes with enhanced mechanical resistance for ultrafiltration application, *J. Eur. Ceram. Soc.* 40 (15) (2020) 5959–5966.
12] H.R. Shan, X.Q. Wang, F.H. Shi, J.H. Yan, J.Y. Yu, B. Ding, Hierarchical porous structured SiO_2/SnO_2 nanofibrous membrane with superb flexibility for molecular filtration, *ACS Appl. Mater. Interfaces* 9 (22) (2017) 18966–18976.
[13] L.R.B. Santos, A. Larbot, C.V. Santilli, S.H. Pulcinelli, Study of the selectivity of SnO_2 supported membranes prepared by a sol–gel route, *J. Sol Gel Sci. Technol.* 13 (1) (1998) 805–811.
[14] L.R.B. Santos, C.V. Santilli, A. Larbot, M. Persin, Influence of membrane-solution interface on the selectivity of SnO_2 ultrafiltration membranes, *Sep. Purif. Technol.* 22–23 (1–2) (2001) 17–22.
[15] Y.Q. Dong, J.W. Shao, C.Q. Chen, H. Li, R.X. Wang, Y.W. Chi, X.M. Lin, G.N. Chen, Blue luminescent graphene quantum dots and graphene oxide prepared by tuning the carbonization degree of citric acid, *Carbon* 50 (12) (2012) 4738–4743.
[16] S.J. Xu, F. Li, B.W. Su, M.Z. Hu, X.L. Gao, C.J. Gao, Novel graphene quantum dots (GQDs)-incorporated thin film composite (TFC) membranes for forward osmosis (FO) desalination, *Desalination* 451 (2019) 219–230.
[17] B.B.V. Salzmann, M.M. van der Sluijs, G. Soligno, D. Vanmaekelbergh, Oriented attachment: From natural crystal growth to a materials engineering tool, *Acc. Chem. Res.* 54 (4) (2021) 787–797.
[18] Y. Liu, Y. Jiao, Z.L. Zhang, F.Y. Qu, A. Umar, X. Wu, Hierarchical SnO_2 nanostructures made of intermingled ultrathin nanosheets for environmental remediation, smart gas sensor, and supercapacitor applications, *ACS Appl. Mater. Interfaces* 6 (3) (2014) 2174–2184.
[19] H.K. Wang, A.L. Rogach, Hierarchical SnO_2 nanostructures: Recent advances in design, synthesis, and applications, *Chem. Mater.* 26 (1) (2014) 123–133.
[20] P. Puhlfürß, A. Voigt, R. Weber, M. Morbé, Microporous TiO_2 membranes with a cut off 500 Da, *J. Membr. Sci.* 174 (1) (2000) 123–133.
[21] T.F. Kuznetsova, A.I. Rat'ko, S.I. Eremenko, Synthesis and properties of porous silica obtained by the template method, *Russ. J. Phys. Chem. A* 86 (10) (2012) 1618–1622.
[22] C. Xu, C. Wang, X.P. He, M.Q. Lyu, S.C. Wang, L.Z. Wang, Processable graphene oxide-embedded titanate nanofiber membranes with improved filtration performance, *J. Hazard. Mater.* 325 (2017) 214–222.
[23] W.H. Park, S.G. Park, M. Kang, M.S. Hyun, N. Choi, D.H. Kim, J. Choo, Direct visualization of a surface-enhanced Raman spectroscopy nano-gap *via* electrostatic force microscopy: Dependence on charge transfer from the underlying surface nano-gap distance, *Appl. Surf. Sci.* 479 (2019) 874–878.